Environ. Sci. Technol. **2005**, *39,* 8142−8149

Fluorescence Spectroscopy Reveals Ubiquitous Presence of Oxidized and Reduced Quinones in Dissolved Organic Matter

ROSE M. CORY* AND
DIANE M. MCKNIGHT
The Institute of Arctic and Alpine Research and Civil and Environmental Engineering, University of Colorado, Boulder, Colorado

Excitation−emission matrixes (EEMs) of 379 dissolved organic matter (DOM) samples from diverse aquatic environments were modeled by parallel factor analysis (PARAFAC). Thirteen components likely representing groups of similarly fluorescing moieties were found to explain the variation in this data set. Seven of the thirteen components were identified as quinone-like based on comparison of their excitation and emission spectra to spectra of model quinones. These quinone-like fluorophores were found to vary in redox state and degree of conjugation. Two components were identified as amino acid-like based on comparison to tyrosine and tryptophan fluorescence spectra. The other four components are not yet associated with any class of molecules. The quinone-like fluorophores account for about 50% of the fluorescence for every sample analyzed, showing that quinone-like fluorophores are an important and ubiquitous fluorescing moiety and in natural waters. Further, the distribution of the quinone-like fluorophores was evaluated as a function of environmental and laboratory redox gradients. Under reducing conditions, the contribution of the reduced quinone-like fluorophores increased concurrent with a decrease in the oxidized quinone-like fluorophores, indicating that DOM fluorescence is a function of redox state of quinone-like moieties. Lastly, a ratio of two quinone-like fluorophores was found to explain the variation in the fluorescence index. These results provide new insight into the redox reactivity of DOM and have implications for the application of fluorescence spectroscopy as a tool to characterize DOM.

Introduction

Dissolved organic matter (DOM) is a heterogeneous mixture resulting from the breakdown of bacterial, algal, and higher plant organic material. DOM plays many significant roles in natural and engineered systems. In aquatic ecosystems DOM controls light attenuation, influences metal speciation and bioavailability, serves as a source of carbon and nutrients to the aquatic food web, and acts as a pH buffer (*1*, *2*). In addition, DOM is a known source of disinfection byproducts during drinking water treatment (*3*). Among the major DOM fractions, the ability of humic and fulvic acids to form complexes with trace metals and attenuate light have been well studied (*1*, *2*). Recently, discoveries on the redox reactivity of fulvic and humic acids have illuminated new mechanisms in which DOM can influence the cycling of metals and organic matter in anoxic environments (*4*, *5*).

The electron-shuttling ability of humic and fulvic acids has been attributed to quinone moieties (*6*−*8*). Quinones are a versatile class of biomolecules found in living cells, in extracellular material, and in detrital organic material. Quinones can cycle between three redox states: oxidized, semiquinone radical, and the reduced, or hydroquinone state (Figure 1). Inside cells, quinones function as electron shuttles and pigments (*9*−*11*). Microbes can produce extracellular quinones to shuttle electrons to terminal electron acceptors such as ferric iron or fulvic acids (*5*, *12*). In addition, quinones can be produced by oxidation of lignin (*13*).

There are multiple lines of evidence for the role of quinones in the redox reactivity of DOM. Electron spin resonance spectroscopy (ESR) studies on DOM fractions have concluded that the observed peaks are due to semiquinone radicals (*6*, *8*). Further, the semiquinone radical concentration increased after microbial reduction for a suite of fulvic acids, showing that the microbial reduction of fulvic acids proceeds via electron transfer to oxidized quinones (*6*). Nurmi and Tratnyek (*7*) found that the redox potentials of different fractions of DOM in nonaqueous solution were qualitatively similar to model quinones. Lastly, laboratory studies have shown that DOM functions similarly to model quinones by comparing their electron-shuttling abilities in laboratory studies (*4*, *12*).

The fluorescence spectra of DOM and isolated fulvic acids contain prominent "humic" peaks that are similar among freshwater and marine samples, despite the inherent chemical heterogeneity and the large pool of potential fluorophores in DOM precursor material (*14*). Differences in the intensity and position of these humic peaks have been correlated with source of DOM; however, the moieties responsible for these peaks have not yet been identified (*15*). For example, the fluorescence index (FI), which is a ratio of emission intensities at an excitation of 370 nm, has been strongly correlated to the relative contribution of microbial versus higher plant-derived organic matter to the DOM pool (*15*). Recent studies indicate that some DOM fluorophores are a function of redox state, suggesting a link between some fluorophores and redox active quinones in DOM (*16*, *17*). In the latter studies, shifts in fulvic acid fluorescence spectra were observed as a function of redox gradients in the field or due to microbial reduction of fulvic acid samples.

Quinones show shifts in UV−vis and fluorescence spectra upon a change in redox state. Consequently, absorbance and fluorescence have been used to detect the presence and redox state of quinones (*18*). The reduction of quinones is generally accompanied by increased intensity of the $\pi-\pi^*$ transitions, especially in the visible range (*19*). This shift explains the darker or more intense color of reduced quinones. Although most unsubstituted, oxidized quinones are not expected to exhibit fluorescence in solution due to efficient intersystem crossing to the triplet state (*20*), many substituted and reduced forms of the parent quinone fluoresce strongly (*21*). The spectral shifts associated with changes in redox state of both quinones and DOM suggest that quinones contribute to the optical properties of DOM. Further, charge-transfer complexes between quinones and hydroxyl aromatics have been proposed to explain the long wavelength absorption tail characteristic of DOM, providing further evidence for the role of quinones in the optical properties of DOM (*8*, *22*).

* Corresponding author phone: (303)492-4687; fax: (303)492-6388; e-mail: Rose.Cory@colorado.edu.

10.1021/es0506962 CCC: $30.25

Published on Web 09/29/2005

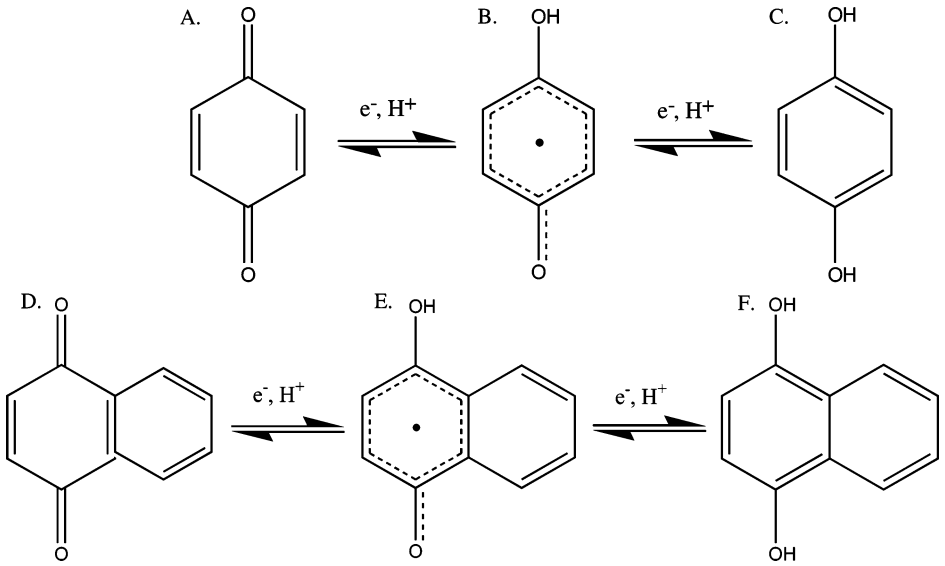

FIGURE 1. One-electron reduction of oxidized quinone to the semiquinone, followed by the reduction of the semiquinone to the hydroquinone. A−C: reduction of benzoquinone; D−F: reduction of naphthoquinone.

The purpose of this study was to evaluate the contribution of quinone moieties to the fluorescence of DOM. We applied parallel factor analysis (PARAFAC, ref 23), a statistical modeling approach, to DOM excitation−emission matrixes (EEMs) of whole water samples and isolated fulvic acids from diverse aquatic environments, including reducing zones of lakes. This analysis allowed us to resolve the EEMs into fluorophores characterized by unique excitation and emission curves. We compared the DOM fluorophores with model quinones and characterized the shift in DOM fluorophores as a function of redox gradients in the environment and in the laboratory. Our results show quinone-like fluorophores of varying redox state are important and ubiquitous DOM fluorophores. Further, the relative amount of these fluorophores shifts consistently as a function of reducing conditions in both laboratory and field settings.

Materials and Methods

Site and Sample Descriptions. The samples included in the PARAFAC analysis fall on the continuum between microbial and higher plant-derived end members. The average fluorescence indices of the sample sets modeled ranged from 1.31 for the Arctic samples to 1.66 for the samples from the McMurdo Dry Valleys, Antarctica (see the Supporting Information). The samples cover a range of aquatic environments. Detailed site descriptions are provided for Nymph Lake and Lake Fryxell where changes in DOM fluorescence across strong redox gradients were studied. A general description of the Arctic site, where nearly one-third of the samples were collected, is also provided.

Lake Fryxell is located in the McMurdo Dry Valleys of Antarctica and is studied by the McMurdo Dry Valleys LTER project (http://huey.colorado.edu/). Because there are no higher plants in the lake basins, the fulvic acids originate from production and degradation of algae and bacteria in the streams and lakes (*17*). Lake Fryxell has a permanent ice cover 5 m thick, and below that the upper water column is saturated with oxygen. A sharp oxycline occurs near 9.5 m, below which the E_h potential decreases steadily with depth. Samples from Lake Fryxell were collected during the austral summer seasons of 2001−2002. Protocols for the microbial reduction of isolated fulvic acids from Lake Fryxell have been described elsewhere (*4*, *17*).

Nymph Lake is a subalpine lake located in Rocky Mountain National Park, CO. Nymph Lake DOM is derived from higher plant and microbial organic matter. During the winter season, reducing conditions prevail in the water column due to ice cover and loss of gas exchange with the atmosphere (Cory, unpublished data). Data collected from winter through spring of 2001−2002 and 2002−2003 showed that the dissolved oxygen (DO) concentration and E_h potential decrease under conditions of ice-cover from December−April. In February, 2003 the ratio of ferrous to ferric iron was greater than 1.0, and in March 2003, the DO concentration was undetectable. In May, the lake iced started to melt, and by June, the lake was ice-free, well mixed, and saturated with DO. When Nymph Lake is covered with ice, inputs of terrestrial DOM to the lake are minimal. Consequently, changes in Nymph Lake DOM under the ice are due to processes acting on the DOM present at the onset of ice cover. During snowmelt, flushing of soil organic matter brings a different pool of DOM into Nymph Lake.

The Arctic LTERs field research site is based at University of Alaska's Toolik Lake field station, Alaska, located in the northern foothills of the Brooks Range (http://ecosystems.mbl.edu/ARC/). Toolik Lake field station is characterized by continuous permafrost, 24 h of sunlight during the summer growing season (May−August), and periods of limited daylight to complete darkness during the winter (Sept−April). Lake ice-out and snowmelt generally occur in May or June. Tussock tundra is the dominant vegetation, but areas of wet sedge tundra, drier heath tundra on ridge tops, and well-drained sites containing river bottom willow communities can be found around Toolik Lake field station. DOM in the surface waters around the Arctic LTER have a low FI (Table 1), suggesting the DOM pool is dominated by higher plant precursor material (*15*). Water samples were collected at the Arctic LTER after snowmelt in June of 2002 and 2003.

Other samples included in this study come from the Niwot Ridge LTER (http://www.lternet.edu/sites/nwt/), the Okavango Delta in Botswanna (*24*), and the University of Notre Dame Environmental Research Center in Michigan (*25*).

Sample Preparation. Four types of DOM samples were included in the data set: whole water, fulvic acids, the hydrophilic fraction, and ultrafiltered DOM. "Whole water" refers to water samples that have been filtered through a 0.45 μm glass fiber filter. The fulvic acid fraction refers to DOM that has been isolated using the XAD-8 chromatographic method (*26*), and the hydrophilic fraction refers to the fraction that passes through the XAD8 column (*26*). Three DOM samples isolated by ultrafiltration (1000 Da cutoff) were also included in this study.

TABLE 1. Comparison of Model Quinone Absorption and Excitation Peaks to Excitation Peaks ofQuinone-Like Components[a]

quinone	benzenoid $\pi-\pi^*$	quinonoid $\pi-\pi^*$	quinonoid $\pi-\pi^*$	benzenoid $\pi-\pi^*$	quinonoid n$-\pi^*$
1,4 benzoquinone[b]		246	288		439
1,4 naphthoquinone[b]	**245**	257 (sh)	340−450[c]	335	425
anthraquinone[d]	**243**	263	320	332	405
Model Quinone Excitation Maxima in Water, Grouped by Wavelength Range[e]					
AQDS excitation	≤**240**	**258** (280 sh)	328		
AHDS excitation	≤**240**	**267**		345(sh)	367
lawsone	**240**		300	340 (sh)	
juglone	**250**			335	
List of Maxima for Quinone-Like Components, Grouped by Wavelength Range					
Q1		**260**	290−320	340[f]	
Q2	≤**250**	280	320[f]		
Q3	≤**250**	280	300	345[f]	
SQ1		260 (sh) **295**		345[f]	380
SQ2		**270**			380
SQ3		265		345[f]	g
HQ	≤**250**	265			≥400

[a] Model quinone data from Berger (*30*). Most intense peak is in bold; sh = shoulder. [b] Solvent = $CHCl_3$. [c] This peak is normally obscured by the second benzenoid transition. [d] Solvent = ethanol. [e] Excitation spectra obtained from EEM; excitation peaks chosen from emission maxima. [f] Benzenoid and quinonoid transition assignments for model quinone absorption peaks only and are for comparison to quinone and component excitation spectra. Because excitation is monitored at the emission maximum, it is not possible to assign peaks to possible transitions. For example, only very minor excitation peaks were observed at wavelengths greater than 400 nm for any model quinone, likely due to the low probability of fluorescence emission from an n$-\pi^*$ transition.

Model quinones (AQDS and lawsone; Sigma-Aldrich) were used without further purification. AQDS was electrochemically reduced to AHDS with H_2 in the presence of a Pd/C catalyst. Fulvic acid and model quinone solutions were dissolved in MilliQ water (18 MΩ), stirred for several hours, and adjusted to near-neutral pH with dilute HCl or NaOH. All quinones and samples collected under reducing conditions were handled (filtered, diluted, transferred to cuvettes) in an inert atmosphere glovebox. EEMs were collected in septa-sealable quartz cuvettes.

Fulvic Acid Characterization with NMR Spectroscopy. Twenty-four fulvic acid isolates included in the data set were analyzed for carbon functional groups using ^{13}C NMR spectroscopy. Solid state ^{13}C NMR spectra were obtained using a ramp cross polarization magic angle spinning (CPMAS) pulse program and two-pulse-modulated decoupling on a Bruker DSX 300 NMR spectrometer, operating at a frequency of 75.48 MHz for ^{13}C (*27*). Functional groups were assigned following Dria et al. (*27*).

Fluorescence Spectroscopy and Modeling. Strongly absorbing samples were diluted in MilliQ-water or in 10^{-5} M bicarbonate buffer to avoid the inner-filter effect (*28*). All EEMs were collected on a Fluoromax-2 or Fluoromax-3 fluorometer (Jobin Yvon Horiba). EEMs were collected every 10 nm over an excitation range of 250−400 nm, with an emission range of 350−550 nm by 2 nm. MilliQ water EEMs were subtracted from each sample EEM. Emission and excitation correction files generated by the Fluoromax manufacturer were applied to each MilliQ-subtracted sample EEM. Intensities were normalized to the area under the water Raman peak (excitation = 350 nm) analyzed daily. Several sample EEMs were collected in triplicate to investigate the reproducibility of the PARAFAC analysis.

The "complete" data set included 379 DOM sample EEMs. PARAFAC statistically resolves EEM data sets of complex mixtures such as DOM into components without making any assumptions on the shapes of the spectra (*23*). Each component identified by PARAFAC has a unique excitation and emission spectrum; however, a component may be a single fluorophore or a group of similar fluorophores. Once the components explaining the greatest variation in the data set are identified, the distribution of components can be calculated for each sample. Split-half analysis was used to validate the identified components following the procedures of Stedmon et al. (*23*).

A McMurdo-only data set was modeled independently to link components to microbial precursor material and to validate combining diverse EEM data sets into one PARAFAC model. The majority of the 73 samples in this data set were collected from Lake Fryxell. The rest of the samples are from other lakes in the McMurdo Dry Valleys.

Spectral Comparisons to Model Quinones. We compared PARAFAC components to published aqueous absorption spectra of model quinones and to fluorescence spectra of model quinones collected for this study. Excitation spectra were evaluated at the wavelength of the emission maximum, which may cause differences between excitation and absorption spectra of model quinones in solution. Due to excited state reactivity, emission can be strongly affected by substituents and the local environment around the fluorophore. Consequently, differences in emission spectra between model and humic quinones are expected, and we relied on relative trends rather than absolute peak positions when comparing emission spectra.

Results

Model Validation. We identified 13 fluorescent components with the PARAFAC model (Figure 2). Comparison of the measured and modeled EEMs for two samples shows that the maximum intensity in the residual EEMs are 2 orders of magnitude lower than the measured EEMs (Figure 3). The residual EEMs show mostly noise, confirming that the PARFAC model accounted for all discernible fluorophores. The two samples presented in Figure 3 represent a microbial end member from Lake Fryxell and a plant-derived end member from Toolik Lake, indicating that the model accurately explains the variation among the EEMs in this data set. Further, the model correctly depicts a broader peak in the Toolik Lake EEM for the longer wavelength peak relative to that of the Lake Fryxell EEM, a feature documented in previous studies (*15*). The hydrophilic fraction samples were the only samples that were poorly explained by the model.

From the triplicate analyses, the reproducibility of percent contribution from each component to the total fluorescence was evaluated. The triplicate EEMs for the same fulvic acid solution had low standard deviations, less than or equal to 1% for each component. For the EEMs collected on measured on different concentrations of the same sample, the standard

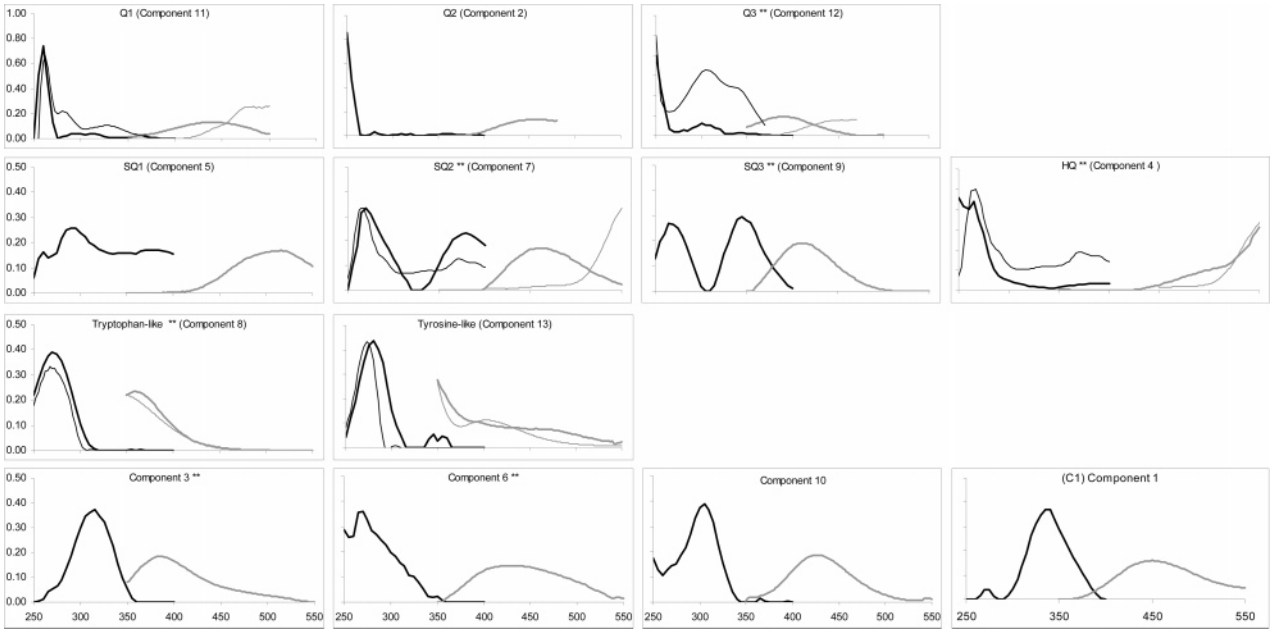

FIGURE 2. Excitation (thick black) and emission (thick gray) curves for the 13 components identified in the total data set. Top row: oxidized quinone-like components. Second row: reduced quinone-like components. Third row: amino acid-like components. Fourth row: unknown components. The component number refers to the order in which the component was identified in the complete model. Components marked ** were identified in a McMurdo-only data set. Intensities are in Raman units. Comparisons to model compounds are plotted in thin lines: Q1 compared to AQDS; Q3 compared to lawsone; SQ2 compared to AHDS; HQ compared to AHDS; C8 compared to tryptophan; C13 compared to tyrosine.

deviation ranged from 0.4% for component seven (C7, SQ2) to 2.8% for component 12 (C12, Q3). The ratio of component C4 (HQ) to C2 (Q2) analyzed in subsequent sections had standard deviations ranging from 0.04 to 0.08.

Identification of Fluorophores. Seven components were identified as quinone-like based on the similarity between number, position, and relative intensities of the component excitation peaks to absorbance and excitation peaks of model quinones (Figure 2; Table 1). The seven quinone-like components accounted for 50−60% of the total fluorescence for all samples. Of the other six components, two resemble amino acid fluorophores, and the remaining four are not yet associated with any class of molecules (Figure 2).

Of the transitions associated with fluorescence, quinones are characterized by intense absorption bands in the range of 250−300 nm, and weaker overlapping bands in the region of 330−400 nm due to quinonoid and benzenoid $\pi \rightarrow \pi^*$ transitions (ref 39; Table 1). Reduced quinones should have increased intensity of fluorescence compared to that of oxidized quinones. Components SQ1, SQ2, SQ3, and HQ are comparable to spectra of reduced quinones such as those shown in Figure 1c,f (Figure 2). SQ1, SQ2, SQ3, and HQ are characterized by excitation maxima around 250−270 and contain appreciable excitation peaks at wavelengths between 330 and 400 nm. The excitation spectra of SQ3, SQ2, and HQ are most similar to AHDS, a model dihydroquinone. AHDS has two strong excitation peaks at low wavelengths: ≤240 (outside our modeling range, not shown in Figure 2) and 265 and another less intense peak at 370 nm. HQ has an excitation maximum less than or equal to 250 nm and another maximum at 265 nm, with a continuous, low intensity excitation "tail" which increases near 400 nm, suggesting that HQ has a longer wavelength ≥400 nm. SQ2 has well-resolved excitation peaks at 270 and 380 nm. SQ1 has distinct excitation peaks at 260 and 295. At wavelengths greater than 295 nm, SQ1 has continuous, broad excitation with a hump around 380 nm, near the longer wavelength excitation peak of AHDS and SQ2. The hump around 380 nm is also where many semiquinones show absorption peaks in aqueous solution (*29*). SQ3 has two equally intense excitation peaks at 265 and 345 nm.

Components Q1−Q3 have intense short wavelength excitation maxima but show minor excitation peaks for wavelengths greater than 300 nm. These components likely represent fluorophores in a more oxidized state, comparable to the structures shown in Figure 1a or d. The most intense excitation maximum of components Q1−Q3 occurs at wavelengths 250−260 nm, in the same range as the low-wavelength maximum of the reduced quinone-like components. The excitation spectrum of Q1 resembles that of aqueous AQDS and the absorption spectrum of anthraquinone in ethanol (ref 30; Figure 2). Q2 and Q3 have excitation peaks that compare well with the absorption spectra of many substituted naphthoquinones or anthraquinones (*30*). Q3 is plotted with lawsone for comparison (Figure 2).

The emission maxima of Q1−Q3 ranged from 440 nm for Q1, to a broad peak from 454 to 460 nm for Q2, and a peak at 388 nm for Q3. The emission peaks of the reduced components are red-shifted relative to components Q1−Q3, except for SQ3 which has an emission maximum at 412 nm. Likewise, AHDS has a red-shifted emission peak compared to AQDS (ref 16; Figure 2). SQ1 and SQ2 have emission peaks at 462 and 520 nm, respectively. The emission peak intensity is greater for the reduced quinone-like components compared to those of Q1−Q3, with HQ showing the most intense emission peak. Further, the emission spectra of AHDS and HQ closely overlap.

Of the remaining components, components C8 and C13 have excitation and emission spectra that match well with the spectra of tryptophan and tyrosine (Figure 2). The tryptophan and tyrosine-like components have been identified previously (*23*), and peaks of the fluorophores have been correlated with measured amino acid concentrations (*31*). Although C1 has similarly located dual excitation peaks to components SQ1−SQ3, the relative intensity of these peaks is different. Because the longer wavelength excitation maximum at 340 for C1 is more intense than the shorter

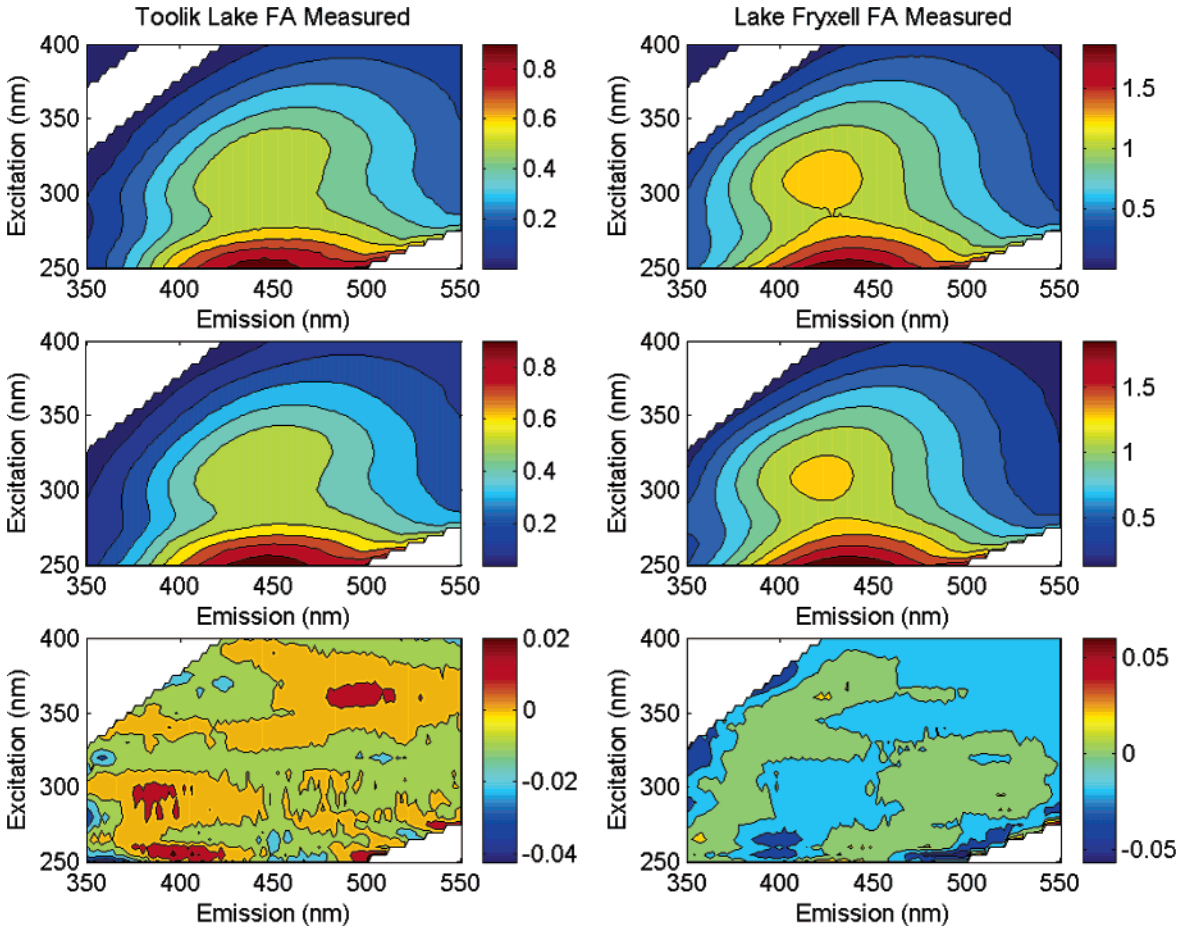

FIGURE 3. Comparison of the measured (top), modeled (middle), and residual (bottom) EEMs for two samples: Toolik Lake fulvic acid and Lake Fryxell fulvic acid. Intensities are in Raman units and are a function of the concentration of the prepared fulvic acid solution. Each contour plot was generated in Matlab using 10 contour lines.

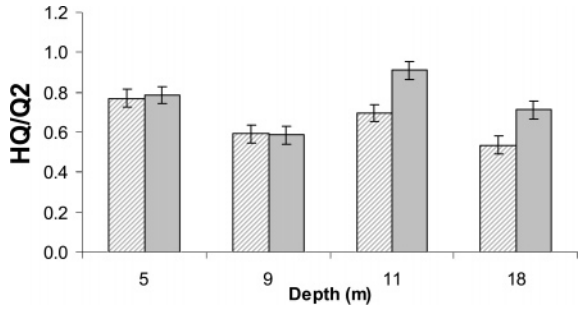

FIGURE 4. Changes in the ratio of HQ/Q2 upon microbial reduction of Lake Fryxell fulvic acids. Error bars in the ratio are the standard deviation in the ratio of HQ/Q2 for three solutions of the same sample run in triplicate.

wavelength peak, C1 did not fit our criteria as quinone-like. C1 and the other three components are not linked with any class of organic molecules (Figure 2).

Components Exhibit Redox Reactivity in Diverse Aquatic Environments. The results of the comparisons based on spectral properties were evaluated in field and laboratory studies. The microbially reduced fulvic acids from two depths below the oxycline in Lake Fryxell showed an increase in the ratio of HQ to Q2 compared to those of the controls (Figure 4). The change in the ratio can be seen by examining the relative contribution of HQ and Q2 (see the Supporting Information). The two fulvic acids from above the oxycline, the 5 and 9 m samples, showed no clear shift in the modeled fluorescence upon microbial reduction.

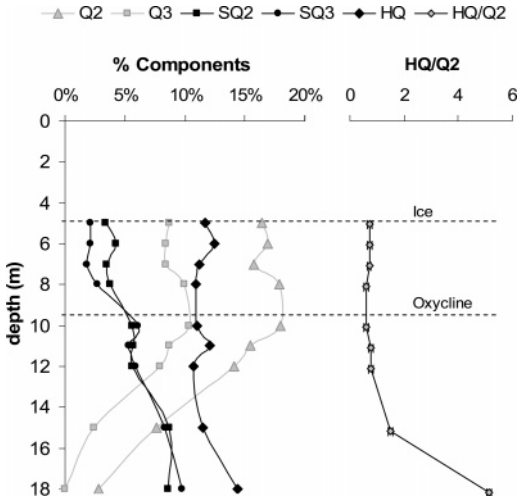

FIGURE 5. Depth profile of quinone-like components from Lake Fryxell whole water EEMs. Side panel: ratio of HQ/Q2. Error bars in the ratio are the standard deviation in the ratio of HQ/Q2 for three solutions of the same sample run in triplicate.

A depth profile of EEMs for whole water samples collected from Lake Fryxell showed that the hydroquinone/semiquinone-like fluorophores HQ and SQ2 increased below the oxycline with a concurrent decrease in Q2 and Q3 (Figure 5). Although these shifts were more pronounced than changes in the fulvic acid fraction upon microbial reduction, they are consistent with those results.

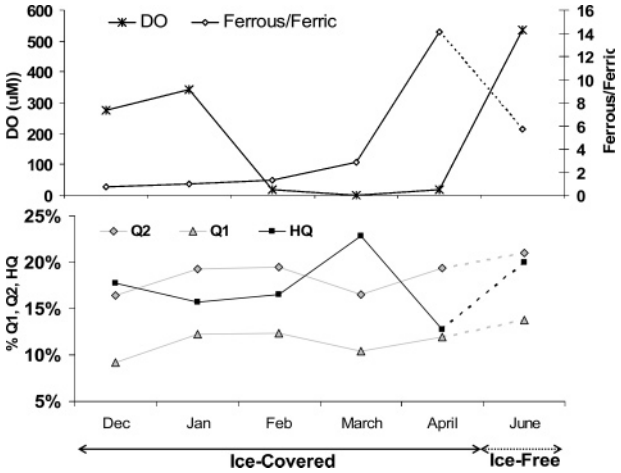

FIGURE 6. Seasonal change in Nymph Lake quinone-like components from whole water EEMs. Top: DO (μM) and ratio of dissolved Fe^{2+}/Fe^{3+}. Bottom: percent of Q1, Q2, and HQ. Dotted lines reflect that the June sample, taken after snowmelt, contains different DOM than the pool of DOM that exists in Nymph Lake during the winter.

A similar change in the distribution of the quinone-like components occurred during ice cover in Nymph Lake. Conditions were most reducing in March in Nymph Lake, exhibiting a decrease in the concentration of dissolved oxygen, an increase in the ratio of ferrous to ferric iron, and a drop in the E_H potential (Figure 6, top, unpublished data). At the same time, the relative contribution of HQ was the greatest in Nymph Lake (Figure 6, bottom). Accordingly, as HQ increased under reducing conditions, both Q1 and Q2 decreased.

Additionally, an intense excitation peak at 230 nm, outside the PARAFAC modeling range, was observed in the EEMs for the reduced Lake Fryxell and Nymph Lake samples (see the Supporting Information). The reduced samples include the microbially reduced fulvic acids and the whole water samples collected below the oxycline in Lake Fryxell, as well as the March Nymph Lake sample. This excitation peak was not present in the control (oxidized) Lake Fryxell fulvic acids, the EEMs from samples collected above the oxycline in Lake Fryxell, or in any of the other Nymph Lake EEMs.

Linking Components to Precursor Organic Matter. Seven of the thirteen components in the complete data set were also identified in the McMurdo-only PARAFAC model linking these components to bacterial or algal origin (Figure 2). The spectral characteristics of these microbial components matched well with those of C8 (tryptophan-like), C3, C6, HQ, SQ2, SQ3, and a combination of Q2 and Q3. Of the quinone-like components, SQ1 and Q1 were not identified in the McMurdo-only data set. However, when the McMurdo samples were modeled in the complete data set, SQ1 and Q1 accounted for 3% and 12% on average of the total fluorescence respectively, similar to the average contributions of 5−11% for SQ1 and Q1 found in all samples.

The fluorescence index (FI) is a ratio of emission intensities which characterizes the slope of the emission curve at an excitation of 370 nm and has been correlated to the relative contribution of microbial versus higher plant organic matter (*15*). A ratio of SQ1 over the sum of SQ1 and SQ2 explained the variation in the FI ($r^2 = 0.84$, $n = 379$; Figure 7). For example, the Toolik Lake samples have a low FI and have higher amounts of SQ1 relative to SQ2; the Lake Fryxell samples show the opposite trend.

Correlations between the ^{13}C NMR data and the PARAFAC components were investigated for isolated fulvic acids. A positive relationship was found between the amount of aromatic carbon and the ratio of components SQ1 and SQ2

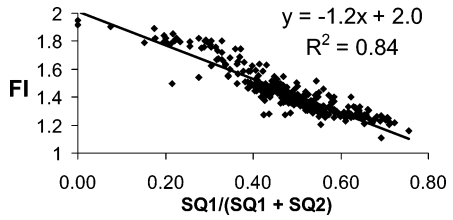

FIGURE 7. SQ1 and SQ2 explain the variation in the fluorescence index (FI). FI = em470/em520 for an excitation wavelength of 370 nm.

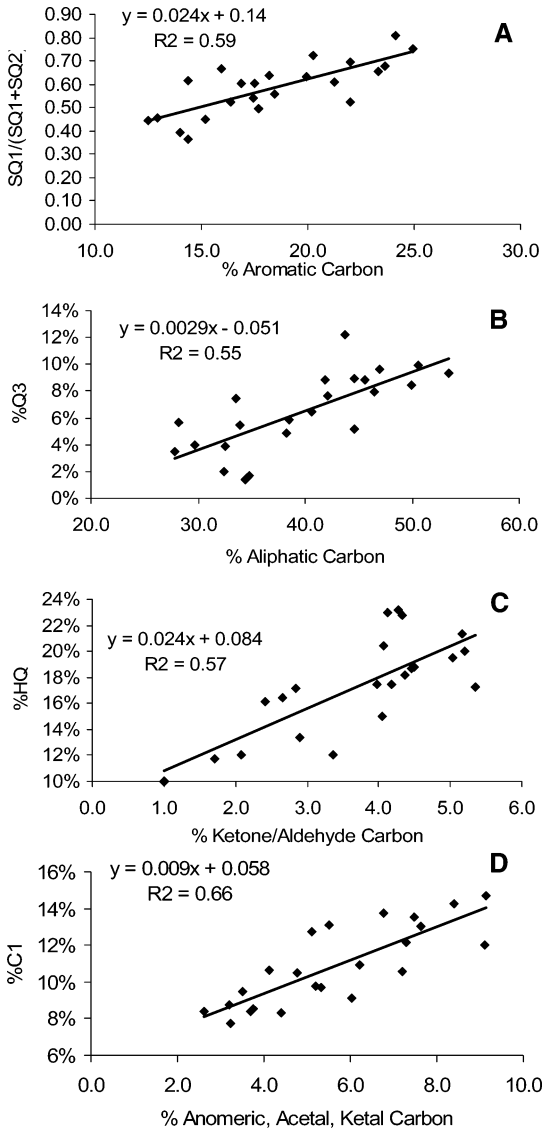

FIGURE 8. Relationships between components and ^{13}C NMR data for fulvic acid samples included in the PARAFAC model. (a) SQ1/(SQ1 + SQ2) vs % aromatic carbon. (b) % Q3 vs % aliphatic carbon. (c) % HQ vs % ketone/aldehyde carbon. (d) % C1 vs % anomeric, acetal, and ketal carbon.

(Figure 8a), indicating that SQ1 is positively related to the aromatic carbon content. A positive correlation was identified between the percent Q3 and the aliphatic carbon (Al-1) content for the fulvic acids (Figure 8b). The percent HQ and the ketone/aldehyde carbon content were correlated (Figure 8c), providing further evidence for the role of quinones (diketones) in DOM fluorescence. Lastly, the amount of carbon detected in the anomeric, acetal, and ketal carbon region was correlated with C1, an unidentified component (Figure 8d).

Discussion

Generally, the differences between the excitation and emission spectra for the oxidized components Q1−Q3 and the reduced components SQ1, SQ2, SQ3, and HQ are consistent with known spectral shifts in model quinones upon reduction. Components indicative of a reduced state are expected to be more fluorescent, with sharper or more intense excitation and emission maxima. All seven of the quinone-like components have similarly located low-wavelength excitation maxima, but the relative intensity of these bands differs among the components. Although HQ, SQ1, SQ2, and SQ3 have less intense low-wavelength excitation maxima compared to components Q1−Q3, they have higher emission intensities. Further, the reduced quinone-like components show increased excitation peaks at longer wavelengths similar to AHDS.

The relationship between HQ and the ketone/aldehyde carbon content provides additional evidence for quinone nature of HQ. The ^{13}C NMR shifts associated with humic quinones may be a function of redox state. Oxidized quinones (diketones) will likely be detected as ketone moieties, and fully reduced quinones may be detected as aromatic carbon.

Field and laboratory studies showed that the quinone-like components are involved in redox reactions, providing biogeochemical corroboration for the presence of redox active fluorophores (*17*, *32*). Reduced components HQ, SQ1, SQ2, and SQ3 account for a greater fraction of fluorescence in reducing conditions in diverse environments, concurrent with decreases in oxidized components Q1−Q3. However, the relative reactivity of these redox active fluorophores may vary between environments, depending upon DOM character and trace metal concentrations. For example, the whole water depth profiles in Lake Fryxell show an increase in HQ, SQ1, SQ2, and SQ3 with depth with a concurrent decrease in Q2 and Q3, with little change in Q1, one of the quinone-like fluorophores that is less important in explaining the variation in microbially derived EEMs compared to the other quinone-like fluorophores. The consistent difference in the EEMs between the microbially reduced and control fulvic acids from Lake Fryxell was an increase in the contribution of HQ. With seasonal shifts in the reducing conditions in Nymph Lake, Q1, Q2, and HQ showed the largest concurrent variation.

SQ1 and SQ2, the two components that account for the fluorescence index, have similar dual excitation peaks, and both appear to be partially or fully reduced quinones, similar to the structures shown in Figure 1b,e. SQ2, however, has better-resolved excitation peaks, in contrast to the broad excitation curve of SQ1. Further, SQ2 has a blue-shifted emission maximum relative to that of SQ1. These data suggest that SQ2 may be in a less-conjugated environment compared to that of component SQ1, consistent with a microbial origin or pool of microbially derived molecules surrounding the fluorophore (*33*). The strong statistical relationship between FI, SQ1, and SQ2 suggests that SQ2 is linked with organic matter of microbial origin.

Additional evidence for the associations of SQ1 with higher plant matter and SQ2 with microbial organic matter was provided by the relationship identified between the ratio of these components and the aromaticity for the fulvic acid samples (Figure 7). Fulvic acid samples containing a large fraction of higher plant-derived organic matter enriched in lignin have higher aromatic carbon fractions (*34*). The relationship between SQ1 and aromaticity supports the correlation between the FI and aromaticity of fulvic acid samples reported by McKnight et al. (*15*).

The broad excitation spectrum of SQ1 is consistent with a higher plant origin and is likely due to overlapping chromophores, which increases the transition probability over a wide range of wavelengths. The position and broad character of SQ1 excitation and emission peaks are consistent with a ground-state charge-transfer interaction proposed by Del Vecchio and Blough (*22*) to explain overlapping absorption bands in plant-derived humic substances. Suggested donor and acceptor molecules for charge-transfer interactions in plant-derived humic substances include hydroxy aromatics and oxidized quinones, respectively, both resulting from lignin breakdown (*15*).

The data suggest that Q3 is also linked to microbial precursor material. A fluorophore similar to Q3 was identified in the McMurdo data set. Further, the percent Q3 was correlated with aliphatic carbon content (Figure 8b). A higher fraction of aliphatic carbon has been correlated with microbial precursor material (*35*). Alternatively, the relationship between Q3 and the aliphatic content could be a function of quenching by some fraction of the nonaliphatic carbon.

The relationship between the anomeric, acetal, and ketal carbon region of the ^{13}C NMR with the amount of C1 suggests that C1 may be a quinone derivative, specifically a ketal, formed by the reaction of a quinone with an alcohol. C1 has similar spectral properties to those of both the reduced and oxidized quinone-like components. Yet, C1 was not counted as a redox-active quinone due to differences in the relative intensities of its excitation peaks compared to those of the quinone-like components and the model quinones. Furthermore, C1 did not show any environmental redox reactivity.

The presence of humic quinones is likely influenced by biological processes which produce quinones and by environmental alteration of quinones and quinone-precursor molecules. Microorganisms primarily produce benzo- and naphthoquinones, and fungi produce anthraquinones as secondary metabolites (*9*, *10*, *30*). The plant pool of quinones is more diverse, because plants produce anthraquinones as well as the benzo- and naphthoquinones (*10*). In addition, lignin degradation provides a heterogeneous pool of quinones (*13*). Considering the relative amount of cellular plant-quinones versus lignin production and degradation, lignin-derived quinones may primarily contribute to the plant-derived quinones, such as Q1 and SQ1, the quinone-like components which were not resolved in the McMurdo-only data set. It is likely that quinones linked to microbial or algal precursor material are also altered through "environmental weathering"; however, there is not an abundant pool of microbial precursor material that could generate extra quinones. This "quinone boost" from lignin degradation could account for the greater quinone content and electron-accepting capacity of plant-derived humics relative to that of microbially derived humics (*6*).

Environmental Implications. Quinone-like components contributed to the EEM of every sample, indicating that humic quinone moieties are consistently incorporated into DOM. In addition, the quinone-like components identified in this model are very similar to several components identified previously in PARAFAC models, which were mainly comprised of whole water marine samples (*23*). Consequently, we concluded that quinone-like fluorophores of varying redox state are important and ubiquitous fluorophores in all natural waters. Our results substantiate the role of quinones in the redox reactivity of DOM, which is important for the cycling of metals (*5*) and the breakdown of natural and contaminated organic matter in anoxic environments (*4*, *12*, *36*). These results show that PARAFAC analysis of DOM EEMs can be used as a tool to study redox reactivity of DOM in situ. In addition, these findings may support the use of fluorescence to study the photoreactivity and source DOM (*37*, *15*). Lastly, these results have implications for the use of the fluorescence-quenching technique used to study the binding of PAHs and metals to DOM (*38*).

Acknowledgments

We gratefully acknowledge C. Stedmon, P. Miller, and three anonymous reviewers for helpful comments on the manuscript. Thanks to C. Johanson for help with Matlab and C. Jaros for figure preparation. This work was funded by NSF Grant Nos. DGE-9987607, OPP-0097182, and OPP-9810219.

Supporting Information Available

Includes further information on site and samples descriptions as well as figures showing changes in the modeled and raw EEMs as a function of field and laboratory redox gradients. This material is available free of charge via the Internet at http://pubs.acs.org.

Literature Cited

(1) Mulholland, P. J. In *Interactivity of Dissolved Organic Matter*; Findlay, S. E. G., Sinsabaugh, R. L., Eds.; Academic Press: San Diego, CA, 2003; pp 139−159.
(2) Maranger, R.; Pullin, M. J. In *Interactivity of Dissolved Organic Matter*; Findlay, S. G. E., Sinsabaugh, R. L., Eds.; Academic Press: San Diego, CA, 2003; pp 186−207.
(3) Reckhow, D. A.; Singer, P. C.; Malcolm, R. L. Chlorination of Humic Materials: Byproduct formation and chemical interpretations. *Environ. Sci. Technol.* **1990**, *24*, 1655−1664.
(4) Lovley, D. R.; Coates, J. D.; Blunt-Harris, E. L.; Phillips, E. J. P.; Woodward, J. C. Humic substances as electron acceptors for microbial respiration. *Nature* **1996**, *382*, 445−448.
(5) Davidson, E. A.; Chorover, J.; Dail, D. B. A mechanism of abiotic immobilization of nitrate in forest ecosystems: the ferrous wheel hypothesis. *Global Change Biol.* **2003**, *9*, 228−236.
(6) Scott, D. T.; McKnight, D. M.; Blunt-Harris, E.; Kolesar, S.; Lovley, D. Quinone moieties act as electron acceptors in the reduction of humic substances by humics reducing microorganisms. *Environ. Sci. Tech.* **1998**, *32*, 2984−2989.
(7) Nurmi, J. T.; Tratnyek, P. G. Electrochemical properties of natural organic matter (NOM), fractions of NOM, and model biogeochemical electron shuttles. *Environ. Sci. Technol.* **2002**, *36*, 617−624.
(8) Ariese, F.; van Assema, S.; Gooijer, C.; Bruccoleri, A. G.; Langford, C. H. Comparison of laurentian fulvic acid luminescence with that of the hydroquinone/quinone model system: Evidence from low-temperature fluorescence studies and EPR spectroscopy. *Aquat. Sci.* **2004**, *66*, 86−94.
(9) Bently, R.; Campbell, I. M. In *The Chemistry of the Quinonoid Compounds, Part 2*; Patai, S., Ed.; Interscience: London, 1974; pp 683−736.
(10) Robinson, T. *The Organic Constituents of Higher Plants*, 2nd ed.; Burgess Publishing Co.: Minneapolis, MN, 1967.
(11) Stites, T. E.; Mitchell, A. E.; Rucker, R. B. Physiological importance of quinoenzymes and the O-quinone family of cofactors. *J. Nutr.* **2000**, *130*, 719−727.
(12) Newman, D. K.; Kolter, R. A role for excreted quinones in extracellular electron transfer. *Nature* **2000**, *405*, 94−97.
(13) Muller, U.; Ratzsch, M.; Schwanninger, M.; Steiner, M.; Zobl, H. Yellowing and IR-changes of spruce wood as result of UV-irradiation. *J. Photochem. Photobiol., B* **2003**, *69*, 97−105.
(14) Coble, P. G.; Green, S.; Blough, N.; Gagosian, R. Characterization of dissolved organic matter in the Black Sea by fluorescence spectroscopy. *Nature* **1990**, *348*, 432−435.
(15) McKnight, D. M.; Boyer, E. W.; Westerhoff, P. K.; Doran, P. T.; Kulbe, T.; Andersen, D. T. Spectrofluorometric characterization of dissolved organic matter for indication of precursor organic material and aromaticity. *Limnol. Oceanogr.* **2001**, *46*, 38−48.
(16) Klapper, L.; McKnight, D. M.; Fulton, J. R.; Blunt-Harris, E. L.; Nevin, K. P.; Lovely, D. R.; Hatcher, P. G. Fulvic acid oxidation state detection using fluorescence spectroscopy. *Environ. Sci. Technol.* **2002**, *36*, 3170−3175.
(17) Fulton, J. R.; McKnight, D. M.; Foreman, C.; Cory, R.; Stedmon, C.; Blunt, E. Changes in fulvic acid redox state through the oxycline of a permanently ice-covered Antarctic lake. *Aquat. Sci.* **2004**, *66*, 27−46.
(18) Poulsen, J. R.; Birks, J. W. Photoreduction fluorescence detection of quinones in high-performance liquid chromatography. *Anal. Chem.* **1989**, *67*, 2267−2276.
(19) Babaei, A.; Conner, P. A.; McQuillan, A. J.; Umapathy, S. UV−visible spectroelectrochemistry of reduction products of anthraquinone in dimethylformamide solutions. *J. Chem. Educ.* **1997**, *74*, 1200−1204.
(20) Gorner, H. Photoreduction of 9,10-anthraquinone derivatives: Transient spectroscopy and effects of alcohols and amines on reactivity in solution. *Photochem. Photobiol.* **2003**, *78*, 440−448.
(21) Diaz, A. Absorption and emission spectroscopy and photochemistry of 1,10-anthraquinone derivatives—a review. *Photochem. Photobiol.* **1990**, *53*, 141−167.
(22) Del Vecchio, R.; Blough, N. L. On the origin of the optical properties of humic substances. *Environ. Sci. Technol.* **2004**, *38*, 3885−3891.
(23) Stedmon, C. A.; Markager, S.; Bro, R. Tracing dissolved organic matter in aquatic environments using a new approach to fluorescence spectroscopy. *Mar. Chem.* **2003**, *82*, 239−254.
(24) Mladenov, N.; McKnight, D. M.; Wolski, P.; Ramberg, L. Effects of annual flooding on dissolved organic carbon dynamics within a pristine wetland, the Okavango Delta, Botswana. *Wetlands,* in press.
(25) Pace, M. L.; Cole, J. J.; Carpenter, S. R.; Kitchell, J. F.; Hodgson, J. R.; Van de Bogert, M.; Bade, D. L.; Kritzberg, E. S.; Bastviken, D. Whole-lake carbon-13 additions reveal terrestrial support of aquatic food webs. *Nature* **2004**, *427*, 240−243.
(26) Aiken, G. R.; McKnight, D. M.; Thorn, K. A.; Thurman, E. M. Isolation of hydrophilic organic acids from water using nonionic macroporous resins. *Org. Geochem.* **1992**, *18*, 567−573.
(27) Dria, K. J.; Sachleben, J. R.; Hatcher, P. G. Solid-state carbon-13 nuclear magnetic resonance of humic acids at high magnetic field strengths. *J. Environ. Qual.* **2002**, *31*, 393−401.
(28) Lakowicz, J. R. *Principles of Fluorescence Spectroscopy*, 2nd ed.; Kluwer Academic: New York, 1999.
(29) Rao, P. S.; Hayon, E. Ionization-constants and spectral characteristics of some semiquinone radicals in aqueous solutions. *J. Phys. Chem.* **1973**, *77*, 2274−2276.
(30) Berger, S.; Rieker, A. In *The Chemistry of the Quinonoid Compounds, Part 1*; Patai, S., Ed.; Interscience: London, 1974; pp 163−230.
(31) Yamashita, Y.; Tanoue, E. Chemical characterization of a protein-like fluorophores in DOM in relation to aromatic amino acids. *Mar. Chem.* **2003**, *82*, 255−271.
(32) Miller, M. P.; McKnight, D. M.; Cory, R. M.; Williams, M. W. Biogeochemical role of humic redox reactions in the hyporheic zone of a headwater stream, Green Lakes Valley, Colorado Front Range, United States. Manuscript in preparation.
(33) McGarry, S. F.; Baker, A. Organic acid fluorescence: applications to speleothem palaeoenvironmental reconstruction. *Quat. Sci. Rev.* **2000**, *18*, 1087−1101.
(34) McKnight, D. M.; Hood, E.; Klapper, L. In *Interactivity of Dissolved Organic Matter*; Findlay, S. E. G., Sinsabaugh, R. L., Eds.; Academic Press: San Diego, CA, 2003; pp 71−93.
(35) McKnight, D. M.; Andrews, E. D.; Spaulding, S. A.; Aiken, G. R. Aquatic fulvic acids in algal-rich Antarctic ponds. *Limnol. Oceanogr.* **1994**, *39*, 1972−1979.
(36) Perlinger, J. A.; Kallurer, V. M.; Enkatapathy, R. V.; Angst, W. Addition of hydrogen sulfide to juglone. *Environ. Sci. Technol.* **2002**, *36*, 2663−2669.
(37) Waiser, M. J.; Robarts, R. D. Photodegradation of DOC in a shallow prairie wetland: evidence from seasonal changes in DOC optical properties and chemical characteristics. *Biogeochemistry* **2004**, *69*, 263−284.
(38) Zhao, J.; Nelson, D. J. Fluorescence study of the interaction of Suwannee River fulvic acid with metal ions and Al3+-metal ion competition. *J. Inorg. Biochem.* **2005**, *99*, 383−396.

Received for review April 11, 2005. Revised manuscript received August 25, 2005. Accepted August 29, 2005.

ES0506962